IOP Conf. Series: Journal of Physics: Conf. Series **843** (2017) 012075 doi:10.1088/1742-6596/843/1/012075

Experimental verification of the coming out of the shaft for the ceramic rolls/rollers with shrink fitting system

Y Sano[1], H Sakai[1],G Zhang[1] and N-A Noda[1]

[1]Department of Mechanical and Control Engineering, Kyushu Institute of Technology Sensui-Cho 1-1 Tobata-Ku, Kitakyushu-Shi, Fukuoka, Japan

E-mail: sano.yoshikazu029@mail.kyutech.jp

Abstract. Ceramic rolls/rollers have an advantage in steel strip production because of its high wear resistance and corrosion resistance. The new rolls/rollers consist of a ceramic sleeve and two alloyed steel shafts connected to the sleeve ends only under a small shrink fitting ratio because of the brittleness. However, the alloyed steel shafts may be loosening out from the ceramic sleeve under such low shrink fitting ratio. In the some previous studies have considered the coming out mechanism was considered by the numerical simulation focusing on the displacement and the shear stress at the joint end. This phenomenon should be confirmed without experiment. In this study, therefore, in order to clarify the coming out behavior, rotating bending experiment is conducted for a small roller specimen consisting of a steel sleeve and steel shafts connected by low shrink fitting ratio. Then, it is found that the coming out can be realized in the small specimen.

1. Introduction

Steel conveying rollers are used in the heating furnace (see Figure 1) for producing high-quality steel plates for automobiles. The conventional roller (Figure 2(a)) material is steel with ceramic spray coating on the outside of sleeve. To reduce the temperature, inside of the roller is cooled by water. However the thermal expansion mismatch may exceed the adhesion strength of the ceramic layer and causes failure on the roller surface such as crack, peeling, and wearing [1]. Therefore, the life of the roller becomes quite short.

Figure 2(b) shows a new ceramic roller consisting of steel shaft at both ends and ceramic sleeve having high heat resistance, high corrosion resistance and high wear resistance [2, 3]. Several previous studies suggested that the shrink fitting system may be the most suitable joining method for cylindrical structures to reduce the maintenance time and cost for the shaft replacement [4-8]. However, since only a small shrink fitting ratio can be used because of the ceramic brittleness [9-15], the coming out of the shaft from the sleeve may happen during operation. In our previous studies, therefore, the coming out simulations are performed by using the finite element method [4, 5] for this kind of roll. Suryadi [4] et al conducted 3D model to simulate the coming out but only until N = 5 loading circles because of the large calculation time. Therefore, Xu [5] et al developed 2D model to reduce the calculation time and obtained the results until N = 40 circles or more. Those studies [4, 5] have proved that the coming out behavior can be realized in the 2D and 3D simulations.

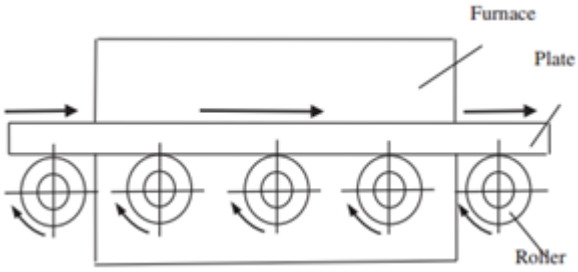

Figure 1 Layout of rollers in heating furnace

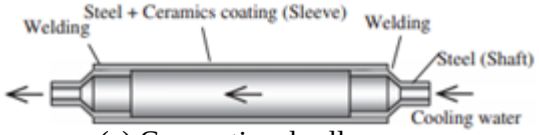

(a) Conventional roller

(b) New roller

Figure 2 Roller structure

However, in the previous studies, the discussion was simply based on the numerical simulation without experiment. The real ceramic rollers and rolls are very expensive having large dimensions (see Figure 3) and therefore not suitable for confirming the coming out phenomenon.

In this study, therefore, in order to clarify the coming out behavior, rotating bending experiment will be conducted for a small roller specimen consisting of a steel sleeve and steel shafts connected by low shrink fitting ratio.

2. Coming out analysis

2.1. Analytical conditions

Figure 3 shows dimensions of the roller considered whose outer diameter D = 300 mm. Here, the roller consists of ceramic sleeve and steel shaft connected by shrink fitting. The shrink fitting ratio is defined as δ/d, where δ is the diameter difference and d is the inner diameter of the sleeve d = 240 mm. The shrink fitting connection was analyzed in the previous studies [8, 13, 14, 17-20].

In this study, the coming out of the shaft is considered under room temperature because the coming out occurs more easily. When we consider the roller in the shrink fitting ratios is considered in the range $\delta/d = 0.01 \times 10^{-3}$-$4.0 \times 10^{-3}$ at room temperature.

Figure 4 shows the roller rotation under loading where Point A located at the bottom of the shaft moves to the top after rotating 180° as shown in Figure 4(b). To simulate the coming out behavior, the roll rotation is replaced by the shifted load win the circumferential direction on the fixed roll as shown in Figure 5. The roller is subjected to distributed load w = 30 N/mm as the weight of the conveyed steel assuming the shaft ends are simply supported. As shown in Figure 5, the continuous load shifting can be replaced by discrete load shifting with load shift angle θ_0, which is usually used as a standard discretization numerical analysis. The suitable shift angle θ_0 =12° is considered with the numerical results. Here, the initial load position θ_0=0° is corresponding to the number of cycle N = 0, and θ = 360° is corresponding to the number of cycle N = 1.

Due to the symmetry, the half model considered with the total number of element 154,320. The smallest element size at the contact portion between sleeve and shaft is 1.25 mm × 1.25 mm × 6 mm. Static structural analysis is performed to the roller by using MSC Marc Mentat 2011[24] with full Newton–Raphson iterative sparse solver of multifrontal method. In this study, a three dimensional elastic FEM analysis can be applied because the loading condition does not exceed the yielding stress for the steel shaft, and the macroscopic plastic deformation does not appear for ceramics sleeve until failure.

The effect of the torsional load at the contact portion can be ignored because the shear stress $\tau_{r\theta}$ is very small compared to the shear stress τ_{rz} [14]. In contact analysis, it is known that two types of friction models, that is, stick–slip model and bilinear model have good accuracy [24]. However, since the stick–slip model needs large amount of data to determine friction force during repetitive calculation process, in this study the bilinear model is applied where the friction force is

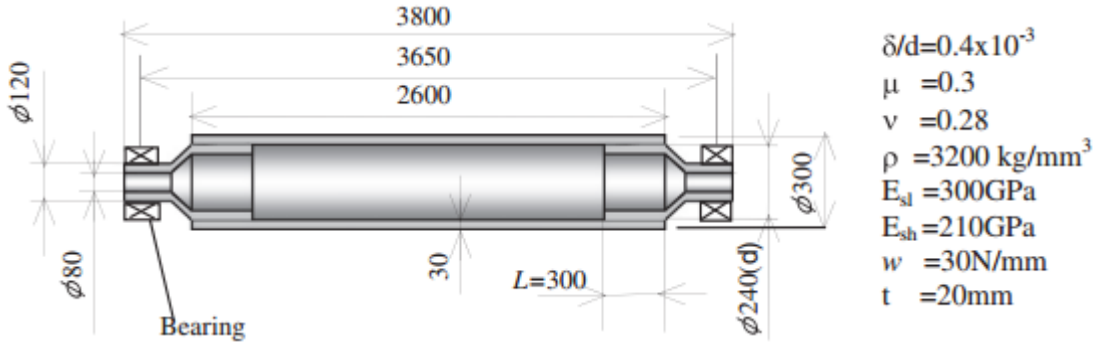

Figure 3 Structure and dimensions of the roller model with standard dimensions (mm)

Table 1 Material properties

Properties	Ceramic	Steel
Young's modulus [GPa]	300	210
Poisson's ratio	0.28	0.3
Tensile strength [MPa]	500	600
Mass density [kg/m^3]	3200	7800
Thermal expansion coefficient [1/K]	0.3×10^{-5}	1.2×10^{-5}

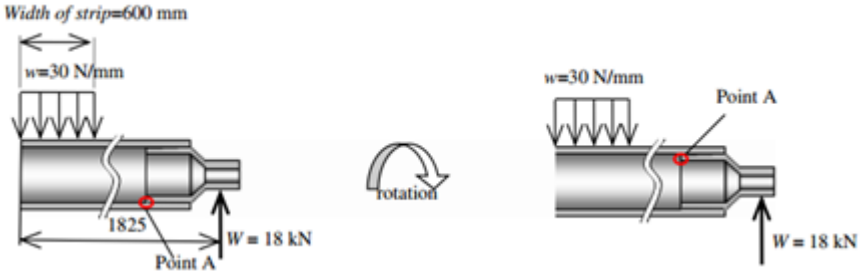

(a) Initial state (b) 180° rotation

Figure 4 Dimensions and loading condition of new roller

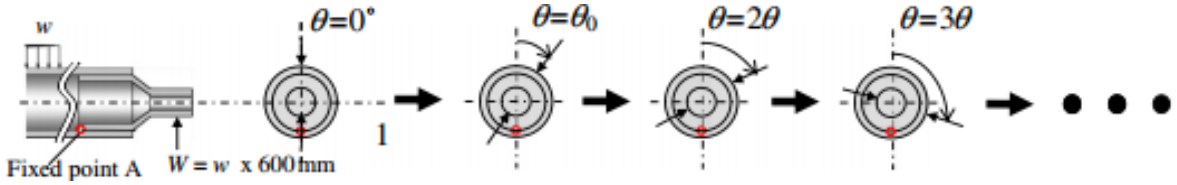

Figure 5 The rotation of the roller replaced by the shifted load at the interval of the load shift angle θ_0. When $\theta = 0°$ the number of cycle $N = 0$, and when $\theta = 360°$ the number of cycle $N = 1$.

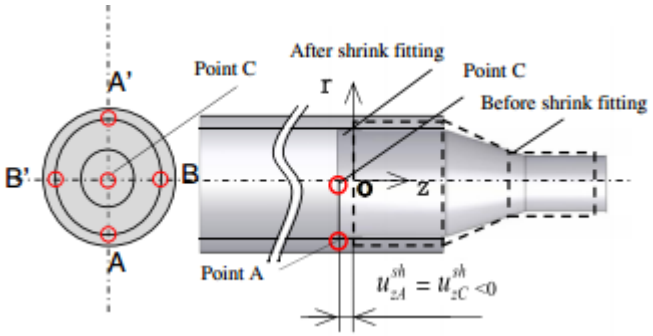

Figure 6 Displacement due to shrink fitting

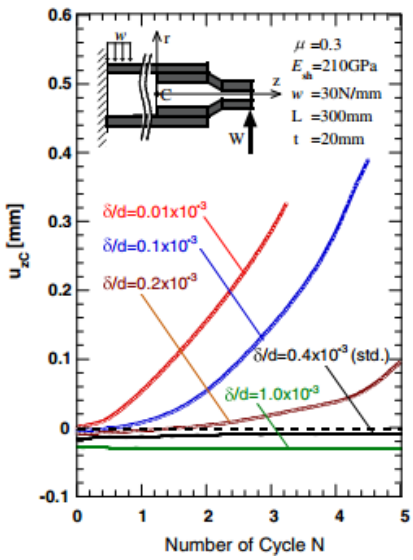

Figure 7 Effect of the shrink fitting ratio on the coming out of the shaft

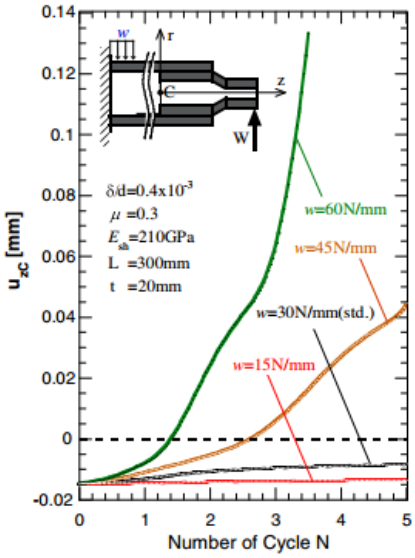

Figure 8 Effect of distributed load on the coming out of the shaft when δ/d=0.4×10^{-3}

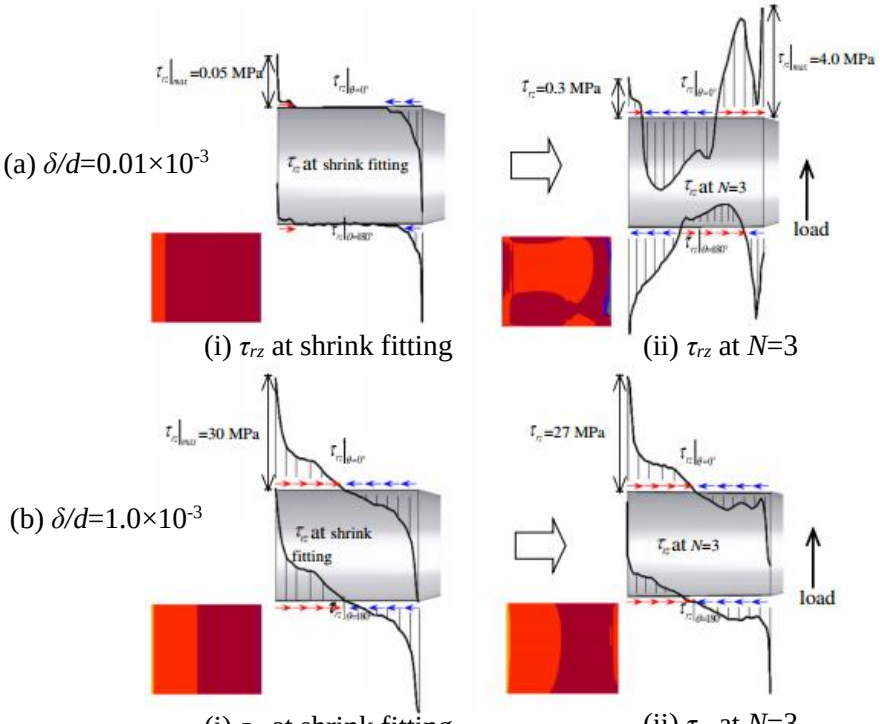

Figure 9 Shear stress distribution τ_{rz} from θ = 180° at shrink fitting and N=3

simply determined from the displacement. The friction coefficient between sleeve and shaft at joint portion is assumed as μ= 0.3. All conditions above are used as a reference condition.

2.2. Analysis result

2.2.1. Effect of mechanical properties on the coming out

Figure 6 illustrates the shaft deformation with the (r, z) coordinate defined before shrink fitting. The displacement u_{zC} in the z-direction is determined from the values at 4 points as $u_{zC}^{sh} = (u_{zA}^{sh} + u_{zA'}^{sh} + u_{zB}^{sh} + u_{zB'}^{sh})/4 = u_{zA}^{sh} < 0$ as shown in Figure 6. Then, since the shaft is under

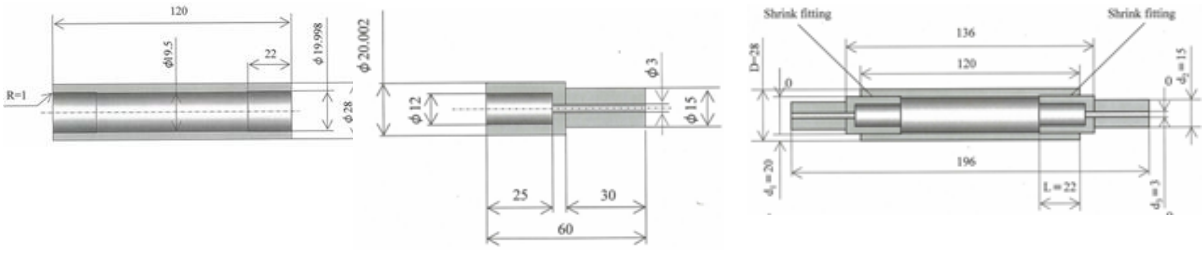

(a) Before shrink fitting (b) After shrink fitting

Figure 10 Dimensions of the sleeve and shaft with shrink fitting ratio δ/d=0.2×10^{-3} used as the test specimen (mm)

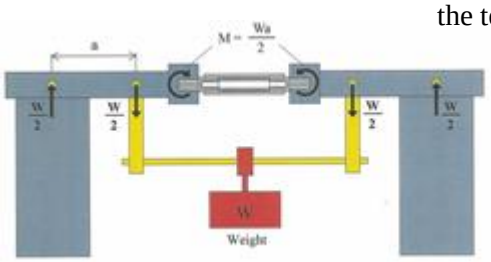

Figure 11 Schematic view of rotating bending machine

Table 2 Specification of gage

GAGE FACTOR	2.23±1.0%
GAGE LENGTH	0.2mm
GAGE REALATANCE	120.2±0.2Ω
ADOPTABLE THERMAL EXPANSION	11.7 PPM/℃

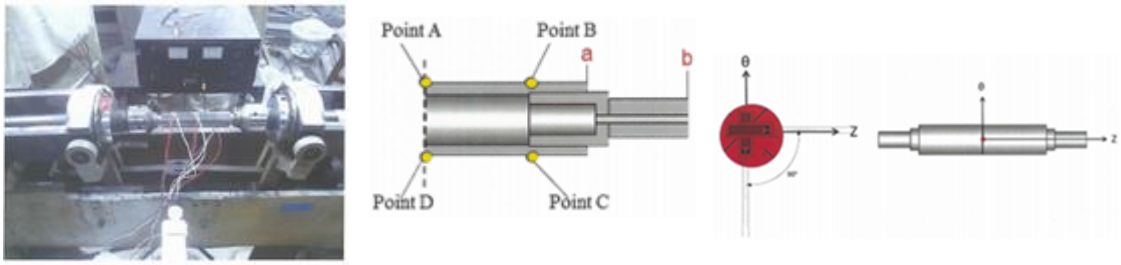

(a) Measurement position (b) Cylindrical coordinate

Figure 12 Strain gauge (KFG-1-120-D-16-11 LIM2S)

compression in the *r*-direction; we have $u_{zA}^{sh} = u_{zC}^{sh} < 0$ Figure 7 shows the results for u_{zC}. With increasing the shrink fitting ratio, the compressive stress increases causing the negative initial value of u_{zC} as shown in Figure 7 at N = 0. Under low shrink fitting ratio, the displacement u_{zC} increases significantly with increasing N.

Figure 8 shows the effects of the magnitude of load is investigated for w = 15, 45, 60 N/mm. The coming out speed significantly increases with increasing the magnitude of the load. It is seen that the coming out accelerates at N = 0–4. In other words, the coming out easily occurs when the distributed load $w \geq 45$ N/mm.

2.2.2. The coming out mechanism

The coming out of the shaft has been realized in the numerical simulation as shown in previous chapters. The results are different depending on the shrink fitting ratio and other parameters. Since it is difficult to obtain the results for large number N because of large calculation time, it is desirable that we can judge the coming out appears or not even when N is small. In this chapter, the coming out mechanism is considered by focusing on the stress distribution appearing at the contact portion.

Figure 9(a) focuses on the stresses along the lines $\theta = 0°$ and 180°. Here, $\tau_{rz}(0)|_{\theta=0°}$ and $\tau_{rz}(0)|_{\theta=180°}$ are compared between N = 0 and 3 under $\delta/d = 0.01 \times 10^{-3}$. The shear stress due to shrink fitting is

Table 3 Comparison of experiment value and FEM value

(a) Comparison of σ_z

		Point			
		A	B	C	D
σ_z [MPa]	Experiment	-101	-88	101	95
	FEM	95	80	107	72

(b) Comparison of σ_θ

		Point			
		A	B	C	D
σ_θ [MPa]	Experiment	-1.6	-4.8	1.6	1.3
	FEM	-1.3	-4.4	1.3	1.1

approximately equal to zero except at both ends when $N = 0$. Therefore, when $N = 3$, the shear stress at shrink fitting is greatly changed, and the shear stress directions are reversed at both shaft ends.

The shear stress at the left end tries to prevent the coming out of the shaft. In Figure 9(b), $\tau_{rz}(0)|_{\theta=0^\circ}$ and $\tau_{rz}(0)|_{\theta=180^\circ}$ are compared between $N = 0$ and $N = 3$ under $\delta/d = 1.0 \times 10^{-3}$. When N=0, it is seen the maximum value $\tau_{rz}|_{max}$= 30 MPa is about 600 times larger than the maximum value $\tau_{rz}|_{max}$= 0.05 MPa in Figure 9(a). Although not indicated, the maximum compressive stress in Figure 9(b) is about 180 times larger than the maximum compressive stress in Figure 9(a). Due to those large shrink fitted stresses, as shown in Figure 9(b), the effect of the bending load becomes smaller and stress does not change very much between $N = 0$ and $N = 3$ under $\delta/d = 1.0 \times 10^{-3}$.

3. Experiment verification to confirm and discuss by using small specimen

3.1. Specimen shape and dimensions

The material of small roll specimen is steel and the shafts are connected to the sleeve end by shrink fitting. Figure 10(a) shows dimensions of the sleeve and shaft before shrink fitting and Figure 10(b) shows dimensions of the roll specimen after shrink fitting. In this experiment we assumed the same value shrink fitting ratio δ/d=0.2×10^{-3}of real ceramic roll (see chapter 2.1). Figure 11 shows rotating bending machine.

3.2. Stress due to shrink fitting and bending

To confirm the real stress of the specimen, the stresses are measured by using the strain gauge. Figure 12 shows how to measure the stress due to bending and rotating for the test specimen. Figure 12(b) shows the positions A, B, C, D where the strains are measured. Here the stresses σ_z and σ_θ are calculated. Table 3 shows comparison between the experiment and FEM results. From Table 3, it is found that both results are good agreement within 10% error in most case.

3.3. Experiment simulation of coming out by rotating bending machine

The rotating bending test cannot be done at lower rotational speed less than 1800rpm. Therefore, in the experimental simulation, the shaft is rotated by hand to realize the coming out.

Figure13 shows the displacement u_{zc} of the shaft under rotating bending. Figure13(a) shows the results of the left shaft and Figure13(b) shows the results of the right shaft. Here, the distances l_1 and l_2 are measured as the distance between the sleeve end and the shaft end as shown Figure 14(a). Assume the average distance between the sleeve end and the shaft end is $l_{ab} = (l_1 + l_2)/2$. Here, l_{ab0} is the initial distance and l_{ab} is the distance after N cycle. Then the displacement u_{zc} is defined from l_{ab0} and l_{ab} as $u_{zc} = l'_{ab} - l_{ab}$ (see Figure 14(b)).

It is seen that the both displacement $u_{zc\text{-left}}$ and $u_{zc\text{-right}}$ increases in the z-direction with increasing the cycle N, that is, the shaft moves in the coming out direction. Therefore, it is found that the coming out are realized in the small specimen.

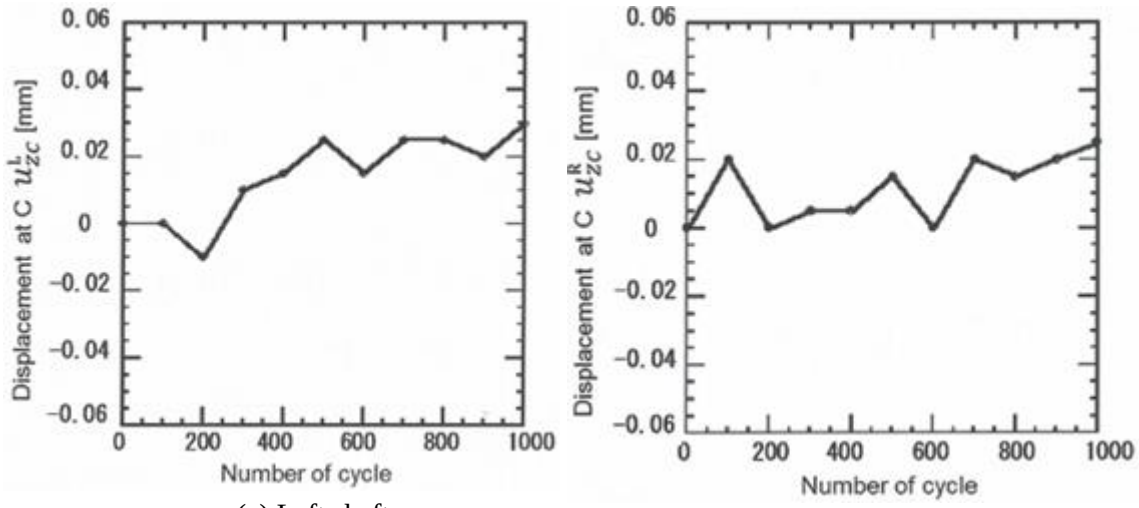

(a) Left shaft (b) Right shaft

Figure 13 The displacement u_{zC} vs. number of cycle

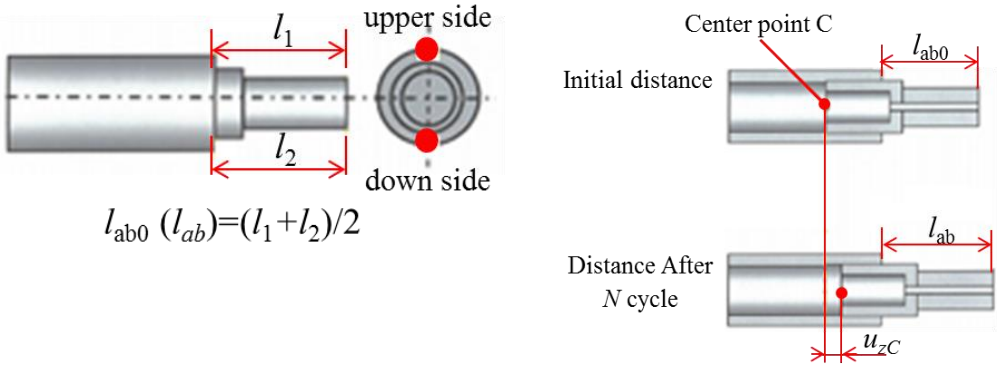

(a) Distances l_1 and l_2 (b) Displacement u_{zc}

Figure 14 Definition u_{zC} and l_{ab0}, l_{ab}

References

[1] M. Fujii, A. Yoshida, J. Ishimaru, S. Shigemura, K. Tani: *Transactions of the Japan Society of Mechanical Engineering* C, 72(2006), 716, 1354-1360.
[2] C. Liour, T. Mori, H. Kobayashi, T. Mitamura: *Journal of the Ceramic Society of Japan*, 98(1990), 4, 348-354.
[3] T. Ono: J. Jpn. Soc. Mech. Eng, 86(1983), 470.
[4] N.A. Noda, D. Suryadi, S. Kumasaki, Y. Sano, Y. Takase: *Engineering Failure Analysis*, 57(2015), 219-235.
[5] N.A Noda, Y. Xu, D. Suryadi, Y. Sano, Y. Takase: Journal of ISIJ International, 56(2016), 2, 303-310.
[6] W. Li, N-A. Noda, H. Sakai, Y. Takase: *Journal of Solid Mechanics and Materials Engineering*, 5(2011), 1, 14-24.
[7] W. Li, N.A. Noda, H. Sakai, Y. Higashi: *Key Engineering Materials*, 452-453(2011), 241-244.
[8] A. Rusin, G. Nowak, and W. Piecha: *Engineering Failure Analysis*, 34(2013), 217-227.
[9] E. Ogawa, K. Shimizu, S. Hamayoshi, N. Kumagai, Y. Ohtsubo, N.A. Noda, Y. Takase, K, Kishi, K. Shobu, T. Tabaru, E, Maeda, S. Koga, T. Matsuda: *Hitachi Metals Technical*

Review, 28(2012), 50.
[10] M. Tsuyunaru, N.A. Noda, Hendra, Y. Takase: *Transactions of the Japan Society of Mechanical Engineering* A, 74(2008), 919-925.
[11] N.A. Noda, Hendra, Y. Takase, M. Tsuyunaru: *Jounal of Solid Mechanics and Materials Engineering*, 2(2008), 11, 1410-1419.
[12] N.A. Noda, Y. Yamada, Y. Sano, S. Sugiyama, S. Kobayashi: Engineering Failure Analysis, 15(2008), 4, 261-274.
[13] N.A. Noda, Hendra, M. Oosato, K. Suzumoto, Y. Takase, W. Li: Key Engineering Materials, 462-463(2011), 1140-1145.
[14] S. Matsuda, D. Suryadi, N.A. Noda, Y. Sano, Y. Takase, S. Harada : *Transactions of the Japan Society of Mechanical Engineering* A, 79(2013), 989-999.
[15] N-A. Noda, D. Suryadi, S. Matsuda, Y. Sano, Y. Takase: *Journal of ISIJ International*, 55(2015), 11, 2416-2425.
[16] Marc Mentat team, Theory and User Information. Vol.A, MSC.Software, Tokyo, 2012.531-596.
[17] N.A. Noda, Hendra, Y. Takase, M. Tsuyunaru: *Journal of Solid Mechanics and Materials Engineering,* 2(2008), 11, 1410–1419.
[18] W. Li, N.A. Noda, H. Sakai, Y. Takase: *Journal of Solid Mechanics and Materials Engineering*, 5(2011), 1,14–24.
[19] W. Li, N.A. Noda, H. Sakai, Y. Takase: *Key Engineering Materials*, 452-453(2011), 241-244.
[20] S. Dedi, N.A. Noda, Y. Sano, Y. Takase, S. Dedi, N.A. Noda, Y. Sano, Y. Takase: *Proceeding of the 4th ACEE 2014*, pp. 221–222.
[21] N.A. Noda, Hendra, M. Oosato, K. Suzumoto, Y. Takase, W. Li: *Key Engineering Materials*, 462-463(2011), 1140-1145.
[22] S. Matsuda, D. Suryadi, N.A. Noda, Y. Sano, Y. Takase, S. Harada: *Transactions of the Japan Society of Mechanical Engineering* A, 79 (2013), 803, 989–999.
[23] A. Rusin, G. Nowak, W. Piecha, Shrink connection modelling of the steam turbine rotor, Eng. Fail. Anal. 34 (2013) 217–227.
[24] Marc Mentat team, Theory and User Information. Vol. A, MSC. Software, Tokyo, 2008. 532.